J Mater Sci (2009) 44:5205–5213
DOI 10.1007/s10853-009-3680-8

FERROELECTRICS

Ferroelectricity in chemical nanostructures: proximal probe characterization and the surface chemical environment

Stephen S. Nonnenmann · Jonathan E. Spanier

Received: 26 March 2009 / Accepted: 11 June 2009 / Published online: 16 July 2009

Abstract Renewed interest in the evolution of the ferroelectric phase transition temperature T_C and the character of ordering of ferroelectric polarizations with finite size and shape is driven in part by several recent developments. An expanding array of pathways for producing nanostructured ferroelectric oxides with control of size, shape, and composition has emerged. Experimental characterization methods originally developed for thin films have been extended to ensemble-free investigations of functional properties of individual nanostructures. Progress in understanding the origin and nature of ferroelectric stability in ultra-thin films and nanostructures is reviewed. Specifically, we discuss evidence for a new surface adsorbate-driven mechanism for stabilizing ferroelectricity in nanostructures owing to a combination of recent proximal probe analysis and model calculation results, along with a new experimental paradigm for investigating and exploiting these effects and effects of finite curvature.

Introduction

In 2009 the outlook for expanding scientific and technological interest in and impact of ferroelectrics is promising, owing in part to recent discoveries and developments involving ferroelectric materials. Intense THz emission [1], an observed high figure of merit in thermocaloric cooling [2], efficient field emission, progress in multiferroic materials for multi-functional properties [3], and advances [4, 5] that can be expected to impact traditional applications are among these developments. Despite progress and intense interest, the concomitant decrease in ferroelectric polarization and evolution of ferroelectric phase transition temperature T_C with finite size due to the destabilizing effects of the depolarizing field, however, continues to pose a significant challenge to achieve further miniaturization and higher integration densities. Recently, comprehensive reviews of planar (thin films) [6] and non-planar (nanotubes, nanowires, nanoribbons) [6–8] geometries have detailed size scaling challenges [2, 9].

Theoretically, the original size scaling models for ferroelectrics proposed by Mitsui and Furuichi [10] and Roytburd [11] have since been adapted many times, with recent revisions including geometric [12] and depolarizing effects [13, 14], and unusual ordering and phase transitions [15]. Fundamental thermodynamic studies, such as those by Ishibashi and Orihara [16], Alpay [17], and Pertsev [18], provide a framework that incorporates the effects of domain wall contributions, stress dependence, and misfit strain between multilayer heterostructures on the stability of the equilibrium polar state, yielding proper mechanical boundary conditions. Interfacial electrostatic effects, such as the contributions of mobile and space charge carriers [19] toward the ferroelectric response in ferroelectric nanostructures, have also been observed via combined theoretical/experimental studies [20], and modified Landau–Ginzburg–Devonshire (LGD) theory [20], respectively. Futher, a LDG study done by Safari and Akdogan [21, 22] showed size-dependent behavior of the thermodynamically governed Landau coefficients, size-induced phase transitions from tetragonal → cubic, and resultant deviations of dielectric and piezoelectric properties from bulk in nanoscale $PbTiO_3$.

In recent years, a number of strategies have been implemented to mitigate the reduction or loss in

S. S. Nonnenmann · J. E. Spanier (✉)
Department of Materials Science and Engineering,
Drexel University, Philadelphia, PA 19104, USA
e-mail: spanier@drexel.edu

ferroelectric polarization in the limit of finite size and the decrease in T_C, or to otherwise manipulate the character of the ferroelectric polarization and/or hysteresis. Among these are the use of strain engineering for enhancing stability and polar properties [23–25] and for inducing a ferroelectric phase in an otherwise paraelectric material [26], and the use of artificial superlattices [27, 28]. A growing body of work on the theoretical foundation for and design use of gradients in strain, composition, and/or temperature to produce ferroelectric polarization gradients, and its practical implementation in thin films has ushered in a new era in functional thin film materials and devices [29]. Recent experimental evidence of room-temperature ferroelectric stability in several-monolayer and single-phase ultra-thin films [25, 30–32] and freely standing nanostructures [33, 34] in the absence of metallic electrodes (an increasingly common and important experimental configuration) [25, 30, 34] has opened a line of inquiry into another potential strategy for engineering ferroelectric stability and increased functionality by harnessing the theoretically predicted and experimentally observed influence of molecular adsorbates on ferroelectric stability.

This review is organized into five sections: following this Introduction, synthetic approaches for producing ferroelectric nanostructures are briefly presented in "Bottom-Up synthesis of ferroelectric nanostructures," followed in "Structural and functional property characterizations of individual $BaTiO_3$ nanowires" by a review of structural and functional property characterizations of individual single-crystalline ferroelectric nanostructures. In "Finite-size evolution of T_C and the influence of surface chemical environment," the results of combining of variable-temperature proximal probe measurements of the diameter-dependent evolution of T_C with infrared spectroscopy and density-functional theoretical calculations including the effects of molecular adsorbates is reviewed and its context among other recent study. Finally, in "Multi-component ferroelectric nanostructures," we remark on and briefly discuss a new approach developed by our group to producing and probing ferroelectric nanostructures, one that is expected to enable further characterization of the effects of finite size, finite curvature, and surface chemical environment.

"Bottom-Up" synthesis of ferroelectric nanostructures

The sub-micron lithographic, ion-beam, and reactive ion etching procedures used in traditional so-called top-down fabrication yield well-defined nanostructures. However, the poor adsorption capacity of high-κ ferroelectrics can lead to damaged and negatively polarized surfaces [35]. Within the last decade, the high demand for increased bit capacity in memory elements and persistent challenges in reducing the sizes of fabricated elements via so-called top-down methods have led to a renewed interest in non-planar, so-called bottom-up synthetic approaches. These latter methods, involving physical- or chemical-vapor deposition or chemical solution means, have been used to produce ferroelectric nanostructures in a range of different shapes and sizes and can involve both template-free [36], and alternately, template-assisted [37] approaches. Template-free heteroepitaxial formation of ferroelectric nanostructures, using physical- and chemical-vapor-phase deposition routes, including sputtering, pulsed laser deposition, and metallorganic chemical vapor deposition, have been employed to produce a range of different nano-structured shapes. The shape evolution is controlled by selection of initial growth mode conditions, namely Volmer–Weber island growth or Stranski–Krastanov layer-to-island growth, and selection of substrate material relating to heteroepitaxial strain and orientation.

Chemical solution-based methods, such as hydrothermal synthesis, sol–gel processing, and solution-phase decomposition, represent an attractive and cost-effective alternative to top-down approaches producing ferroelectric nanostructures for some applications [38, 39]. Some of these routes feature outstanding synthetic control of size and shape [40], and composition [41], particularly in the size range <100 nm. Hydrothermal growth of ferroelectric nanoparticles typically requires low-temperature, high-pressure processing step of extremely basic (pH) aqueous precursor solutions, producing high quality nanocrystalline perovskites without the necessity for a post-anneal heat treatment. Sol–gel processes begin with a stoichiometrically correct quantity of metal alkoxide precursors which then undergoes a controlled hydrolysis sequence finally yielding a stable suspension of nanoparticles. These processes, like hydrothermal growth, occur at relatively low temperatures (<200 °C), depending upon the stabilizing agent used during hydrolysis. Unlike hydrothermal growth, however, sol–gel nanoparticle powders require calcination to obtain the correct structural (and ferroelectric) phase. In solution-phase decomposition, a moisture-sensitive single bimetallic alkoxide precursor is added to an acid mixture primarily consisting of a stabilizing agent and an alcohol, avoiding premature hydrolysis, where then a small amount of peroxide is added to slowly promote hydrolysis over an extended time window, providing excellent control over size and stoichiometry [33, 40, 41]. The as-synthesized nanoparticles are of perovskite structure and require no post-growth thermal treatment. These methods, coupled with dielectrophoresis or other methods of assembly, may permit controlled placement on and integration of ferroelectric nano-particles with non-traditional substrates.

A significant barrier to application of bottom-up synthetic approaches relates to scalability, e.g., the need to precisely locate ferroelectric nanoparticles on a wafer scale in a manner that is compatible with CMOS and related processes; although, significant progress has been made with other inorganic nanostructures [42]. Since its discovery in 1995 by Masuda and Fukuda [43], the phenomenon self-organization of local etching into hexagonal close-packed arrays of columnar pores during the formation of anodized aluminum oxide (AAO) has been applied to the formation of arrays of nanowires and nanotubes of a wide variety of inorganic materials, including oxide perovskites. One feature of template-assisted growth of oxide perovskite nanowires and nanotubes is the selectable control of nanowire and nanotube diameter and length, achieved via selecting AAO pore diameter and pore length using electrochemical overpotential and length of anodization time [44]. In template-assisted growth, a sol–gel metal alkoxide precursor wets the pore during immersion, with the immersion time dictating the desired topology, i.e., longer times result in nanowires and shorter times in nanotubes [45]. Template-assisted growth of some of the most technologically important ferroelectric perovskite materials: lead titanate, barium titanate, lead zirconate titanate, strontium bismuth titanate, and multiferroic barium ferrite nanowires and nanotubes have been reported, along with their structural and functional characterizations [46–51]. Other template materials have also been employed to produce nanowires and nanotubes, including nanoporous silicon [48, 51] and nanoporous block copolymers [52]. The combined advantages of low-temperature chemical processing and ordered templated-growth to produce high yield arrays of perovskite oxide ferroelectric nanostructures hold significant promise for future miniaturization of nanoscale ferroelectric capacitors [53, 54].

Structural and functional property characterizations of individual $BaTiO_3$ nanowires

The syntheses of well-isolated nanostructures of ferroelectric oxides have traditionally been difficult, in part due to the fact that high-temperature heat treatments inherent to these synthetic methods typically cause nanocrystalline particles to lose their small size. Single-crystalline nanowires composed of $BaTiO_3$ were produced [46] using a modification of a synthetic scheme originally developed and reported by O'Brien et al. [40] to produce well-isolated and monodisperse perovskite nanocrystals of homogeneous composition. Significantly, the synthetic product of these approaches possesses the correct product stoichiometry without high-temperature treatment. The synthesis of $BaTiO_3$ and $SrTiO_3$ nanowires were produced via solution-phase decomposition of barium (alternately strontium) titanium isopropoxide, $BaTi[OCH(CH_3)_2]_6$ ($SrTi[OCH(CH_3)_2]_6$) in the presence of coordinating ligands. Energy-dispersive X-ray analysis of the reaction product confirmed that the nanowires contain stoichiometric amounts of Ba and Ti [46] and transmission electron microscopy (TEM) demonstrated that the reaction product is primarily well-isolated nanowires possessing diameters ranging from less than 5 to 70 nm with lengths ranging from hundreds of nanometer to some exceeding tens of microns, depending upon the total reaction time (Fig. 1). X-ray diffraction analysis of nanowire ensembles confirmed that the nanowires are composed of crystalline $BaTiO_3$; sharp patterns in the converging beam electron diffraction (CBED) are exhibited, consistent with the body-centered

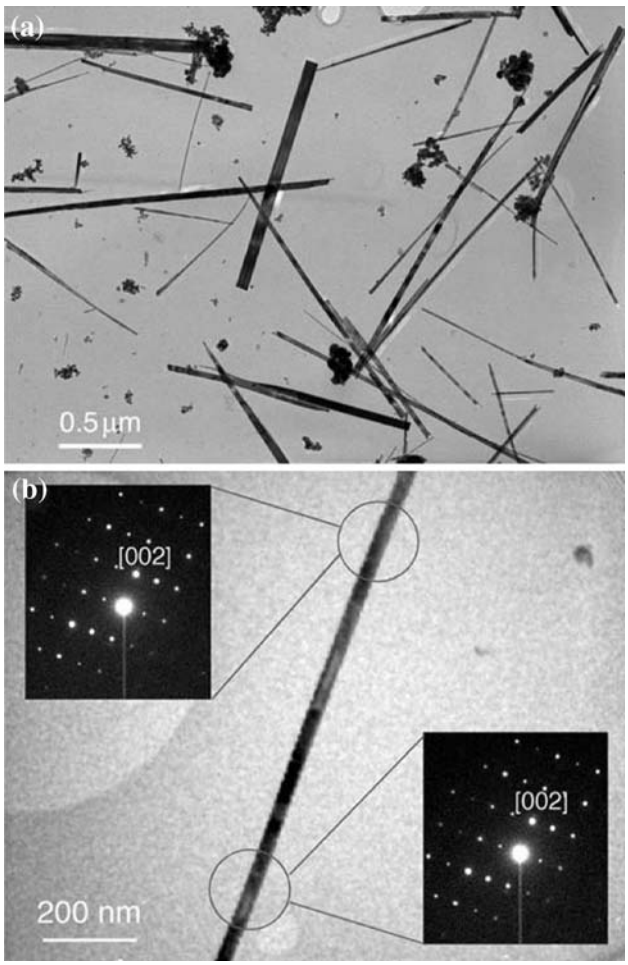

Fig. 1 **a** Transmission electron microscopy (TEM) image of $BaTiO_3$ nanowires showing that the reaction produces mainly nanowires and small quantities (~10%) of nanoparticle aggregates. **b** TEM image of a $BaTiO_3$ nanowire along with two convergent beam electron diffraction (CBED) patterns shown as *insets*. The *circles* represent the region where the CBED patterns are obtained. Analysis of the CBED patterns show that the nanowire is single-crystalline with the [001] direction aligned along the wire axis. Reprinted with permission from Ref. [33]. Copyright 2003 Wiley-VCH

cubic structure with a lattice constant of ~ 4 Å (Fig. 1b, inset). The CBED patterns taken from different positions along the nanowire are found to be identical within experimental accuracy demonstrating that each nanowire is a single crystal.

Having emerged as one of the most valuable means of examining the properties of ferroelectric thin films and patterned nanostructures, scanning probe microscopy (SPM), specifically electrostatic force microscopy (EFM) of individual $BaTiO_3$ nanowires was carried out in ultra-high vacuum using a conductive tip [55]. Compared to other characterization methods such as Raman scattering and X-ray diffraction, SPM has a distinct advantage because it can readily locate individual nanostructures, measure their sizes, and then directly probe and manipulate the ferroelectric polarization. Briefly, the direction of local ferroelectric polarizations within individual nanowires dispersed on a conductive (Au-coated) substrate were individually and independently "written" and manipulated by applying a DC voltage to a conductive tip held at a fixed distance from the nanowire. The resulting written polarizations were probed or "read" using EFM by measuring the shift in the relative phase of the oscillating SPM cantilever tip while applying a smaller DC voltage and scanning at a larger constant-offset distance from the nanowire. Images of collected variations in the phase (or frequency) of the cantilever oscillation during scanning amount to net attractive or repulsive electrostatic interactions between the tip and nanowire. Contrast in an EFM image reflects the variation in the electrostatic potential across the surface of the nanowire arising from the presence of localized surface charges, a finite-range dipole layer, and/or variations in the work function. The EFM images when processed as a subtraction of successive responses collected at probing voltages of opposite polarity represent a spatial map of the local polarization direction in the nanowire. As shown in Fig. 2, successive EFM images of distinct polarization domains written in a 12-nm diameter nanowire demonstrate that multiple nanoscale polarizations can be independently induced and manipulated within a single $BaTiO_3$ nanowire [33]. Pristine nanowires show no discernible EFM contrast, indicating that they do not exhibit an observable polarization with a component perpendicular to the wire axis. The EFM images obtained after the writing procedure demonstrated that a local and stable (>7 days) ferroelectric polarization perpendicular to the wire axis can be induced by an external electric field. As discussed in Ref. [33] nanoscale polarization domains as small as ~ 100 nm^2 in size can be induced on a nanowire, and the ferroelectric nature of a $BaTiO_3$ nanowire can be further probed using the hysteresis characteristics associated with local polarization reversal [33].

Finite-size evolution of T_C and the influence of surface chemical environment

The experimental results in reported in Refs. [33, 34] confirmed, once again, the importance of compensation of polarization-induced surface charges as a stabilizing factor

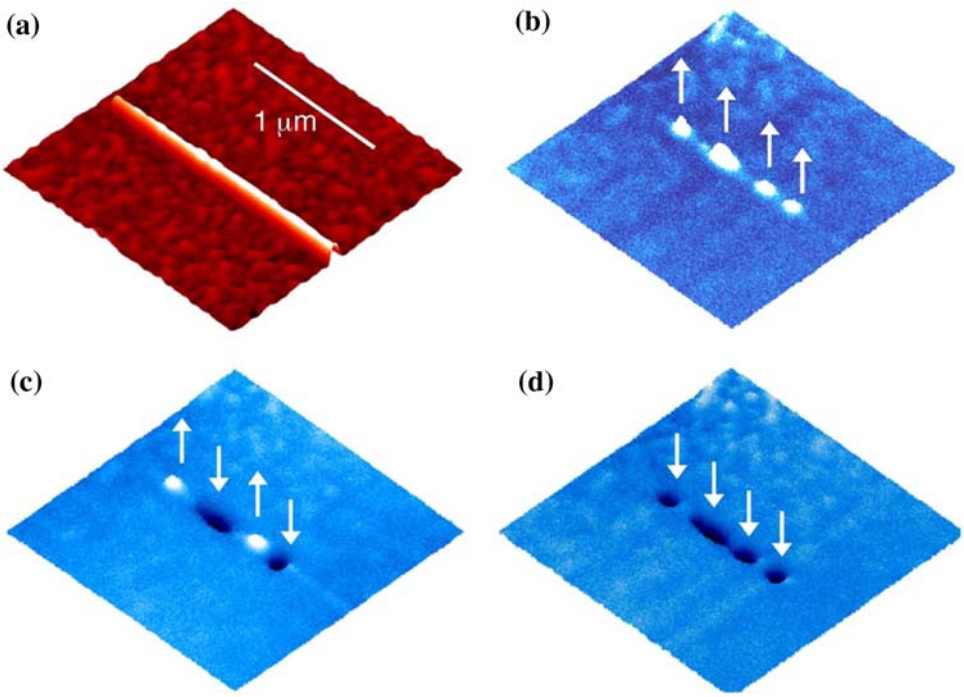

Fig. 2 **a** Topographic image of a 12-nm diameter $BaTiO_3$ nanowire, **b–d** successive electrostatic force microscope (EFM) images showing that four distinct polarization domains can be independently manipulated by an external electric field. In these EFM images, the *bright* and *dark* colors correspond to the resonance frequency shift of $+10$ and -10 Hz, respectively, and the *white arrows* indicate polarization directions. Reprinted with permission from Ref. [33]. Copyright 2003 Wiley-VCH

for ferroelectricity in nano-structures, where incomplete screening of surface charges results in a depolarization field that opposes the bulk polarization, thereby suppressing ferroelectricity. Recently, combined experimental and theoretical investigations involving nanoscale ferroelectricity in single-crystalline $BaTiO_3$ nanowires were performed, resulting in the first demonstration of a new mechanism for the screening of surface charge on ferroelectric nanostructures by atomic and molecular adsorbates.

A variable-temperature SPM study of individual single-crystalline $BaTiO_3$ nanowires possessing diameters ranging from 3 to $\sim$100 nm was undertaken to investigate the finite-diameter evolution of T_C. The nanowires were synthesized using the method presented in Ref. [46], were again dispersed on an Au-coated substrate, and their ferroelectric switching properties were investigated using variable-temperature EFM carried out in UHV (base pressure $\sim 10^{-10}$ torr), following location of each individual nanowire to be probed and measurement of diameter obtained from topographic height scanning. As reported previously, a scheme for inducing, manipulating, and observing the direction of ferroelectric polarizations within the $BaTiO_3$ based on the results of Refs. [33, 34, 55] was employed for this study.

The time variation of the EFM signal from individual nanowires was recorded as a function of temperature for nanowires of diameters from 3 to 50 nm to determine the evolution of the finite-diameter dependence of the ferroelectric phase transition temperature. A series of such images collected for a 25-nm diameter nanowire at two different temperatures is shown in Fig. 3. The signal did not decay over a period of >7 days when the sample was probed at low temperature, indicating that the nanowire was ferroelectric. However, at higher T, the induced polarization was seen to be metastable, decaying with time (Fig. 3), consistent with previously published electrostatic scanning probe characterizations of ferroelectric thin films at temperatures below, near, and above T_C [56]. Temperatures were identified below which the polarization was stable for the duration of the experiment ($\sim$200 h) for each nanowire defining the diameter dependence of the T_C. Shown in Fig. 4 is the decay time scale plotted as a function of $1/k_BT$. We note here that no systematic variation in slope is seen among the data collected from different nanowire diameters.

Measured for the first time in individual nanostructures using a functional probe, the finite-size evolution of T_C on nanowire diameter d_{nw} shows that T_C in larger diameter nanowires is close to $T_{C,bulk}$ ($\sim$400 K) but drops rapidly as d_{nw} decreases. Furthermore, the inset of Fig. 5 shows that the reduction of T_C is inversely proportional to d_{nw}. Notably, T_C reaches room temperature when d_{nw} is $\sim$3 nm, thus establishing the smallest diameter at which a stable polarization signal can be measured at room temperature. With the finite extent of the ferroelectric polarization along the axis of the nanowire to several tens of nanometers, such a volume (<100 nm^3) remains among the smallest volume of ferroelectric polarization reported to date. Extrapolation of the experimental data indicated that nanowires with d_{nw} as small as 0.8 nm can support ferroelectricity at lower temperatures.

The $1/d_{nw}$ scaling relation shown in Fig. 5 suggests that the observed suppression of ferroelectricity is caused by the depolarizing field. However, at the time that Ref. [34]

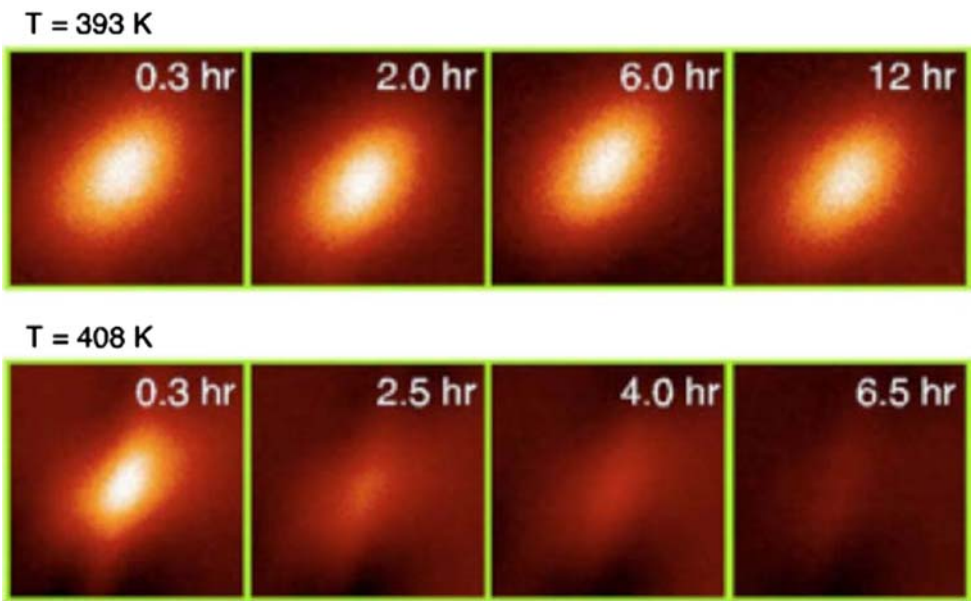

Fig. 3 Time series of EFM images (300 nm × 300 nm) for a 25-nm diameter nanowire following the polarization writing below and above the phase transition temperature. The polarization map was obtained by subtracting the electric force microscope (EFM) response at probing voltages of opposite polarity to remove the contributions from capacitive and topological interactions between the tip and the sample. *White* corresponds to a resonance frequency shift (Δv) of 15 Hz. Reprinted with permission from Ref. [34]. Copyright 2006 American Chemical Society

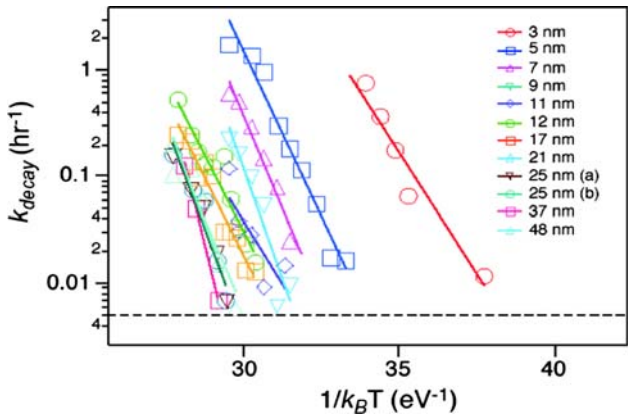

Fig. 4 EFM decay timescale (plotted in reciprocal hours) as a function of $1/k_BT$. The *dashed line* corresponds to 200 h, and is the operational timescale for estimating the ferroelectric phase transition temperature (T_C) in each nanowire. No systematic diameter-dependent variation in the slope of the timescale versus $1/k_BT$ is observed

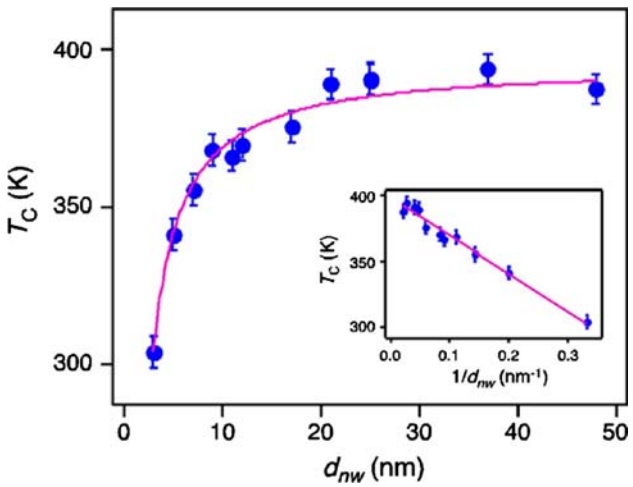

Fig. 5 Ferroelectric phase transition temperature (T_C) as a function of d_{nw}. The *solid circles* denote the experimentally determined T_C. The magenta *solid line* is the result of the fit to the data using the $1/d_{nw}$ scaling relation. Plotted in the *inset* is T_C as a function of $1/d_{nw}$, and illustrates the inverse-diameter dependence. Reprinted with permission from Ref. [34]. Copyright 2006 American Chemical Society

was published, the prevailing view of ferroelectric destabilization with size suggested that the magnitude of this depolarizing field should become too large to support stable polarization at significantly greater values of d_{nw} than those observed in Fig. 5, particularly in a geometry lacking a top metallic electrode to screen the polarization charge. The data therefore suggest that a new screening mechanism is responsible for stabilizing nanoscale ferroelectricity in $BaTiO_3$ nanowires, namely one relating to adsorbate- and/or oxygen vacancy-induced charge screening.

What is the nature of this mechanism? Previous studies had shown that surface hydroxylation is prevalent in oxides, including $BaTiO_3$, especially when these oxides are prepared by wet chemical methods, and that chemisorbed OH is stable in an ultra-high vacuum environment at elevated temperatures (>670 K) [57–59]. Moreover, the $BaTiO_3$ nanowires studied here are covered with oleate ligands that are introduced during the synthesis. Infrared absorption spectroscopy of the nanowire ensemble that underwent high-temperature treatment in ultra-high vacuum confirmed the presence of OH and oleate groups on the surface of $BaTiO_3$ nanowires. These molecular adsorbates can compensate the surface polarization charges, providing a mechanism for reducing the depolarizing fields.

To assess the role of molecular and atomic adsorbates, the $BaTiO_3$ nanowires were modeled via accurate first-principles density-functional-theory (DFT) computations. The reader is referred to Ref. [34] for complete details of the DFT simulations. Briefly, comparison of results for 0.8-nm nanowires and 0.8-nm films revealed only minor differences in adsorbate adsorption energy (0.04 eV) and ionic displacements in the oxide (<0.0025 nm), indicating that ferroelectricity in nanowires and thin films behave similarly. Both BaO- and TiO_2-terminated structures were modeled, and showed very similar adsorbate-stabilized ferroelectricity. The bottom Au electrode was modeled in three different ways; as a vacuum, as a physisorbed film, and as a film forming an epitaxial interface with one $BaTiO_3$ surface. In addition to OH, atomic H and O were also considered as adsorbates, and the effect of the oleate ligands was modeled by the adsorption of HCO and HCOO (products of HCOOH molecules). The favored adsorption site for both OH and O was determined to be directly above the surface Ba or Ti cation, while the H preferred to bind to the surface oxygen ions. The HCO fragment acted as an electropositive adsorbate, bonding to a surface oxygen ion through the carbon atom, while the electronegative HCOO preferred to form an ester linkage with a surface cation.

The results of the simulations demonstrate unambiguously that molecules are dramatically more effective than vacuum or metal electrodes at stabilizing ferroelectricity. In agreement with previous studies, none of the bare $BaTiO_3$ films considered were found to have a stable ferroelectric state; the thinnest $SrRuO_3/BaTiO_3/SrRuO_3$ film with non-zero polarization at $T = 0$ K in a recent study was 3.2-nm (8 unit cells) thick with polarization that is a small fraction of the bulk value. In contrast, the calculations demonstrated that all the $BaTiO_3$/adsorbate systems considered exhibit bulk-like ferroelectricity in even the thinnest films and nanowires. Regardless of the method used to simulate the Au electrode, the electronegative adsorbates (OH, O, HCOO) were seen to stabilize a positive polarization (cations toward the surface), while the

electropositive adsorbates (H, HCO) induce a negative polarization direction (cations away from the surface). A representative structure of a 1.6 nm $BaTiO_3$ film with a full coverage of OH adsorbates is shown in Fig. 6. As seen in the figure, the presence of the OH adsorbates enhances ferroelectricity at the positively polarized surface and maintains a characteristic ferroelectric displacement pattern throughout the film. Similar trends are observed in the other $BaTiO_3$/adsorbate systems, with the ferroelectric displacements enhanced at the $BaTiO_3$/adsorbate interface in all cases. The DFT calculations show that an overlayer of adsorbates stabilizes strong ferroelectricity throughout the nanowires regardless of the presence or absence of an Au electrode. This suggests that atomic or molecular adsorption screens a significant amount of the polarization charge on the surface reducing the depolarizing field relative to bare $BaTiO_3$. The finding from DFT calculations that such an overlayer of adsorbates (whose presence was confirmed by infrared absorption spectroscopy) can stabilize strong ferroelectricity, along with the observation of room-temperature ferroelectricity in 3-nm diameter nanowires is even more compelling in light of first-principles statistical mechanical arguments [60, 61] that were used to demonstrate that OH, O, and H adsorbates are thermodynamically stable under experimental temperatures and pressures. Detailed calculation of the Gibbs free energy for a selected absorption reaction involving OH as a function of temperature at the experimental H_2O and O_2 gas pressures ($p_{H_2O} = p_{O_2} \sim 10^{-12}$ atm) was used to determine the temperature value above which OH adsorption becomes thermodynamically unstable for selected values of film thickness. The film thickness-dependent value of this temperature ranges from 380 to 420 K, higher than the experimental value of T_C at all film thicknesses. While the calculations show that the Gibbs free energy change for O and H adsorption is also favorable under some range of temperature, OH adsorption is the most favorable, indicating that sufficient OH molecules are present in the temperature and pressure range accessed in the experiment, and providing further evidence that OH-induced charge screening is responsible for the observed ferroelectric stabilization.

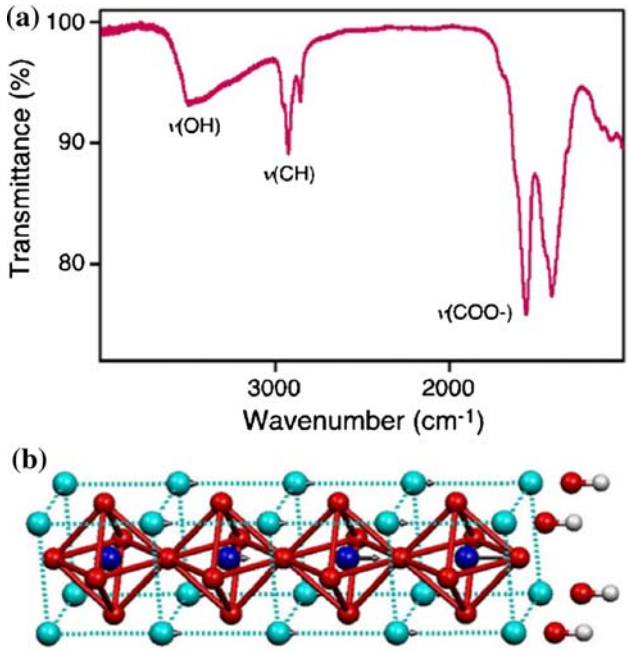

Fig. 6 **a** An infrared spectrum of a $BaTiO_3$ nanowire ensemble showing bands of OH stretching (from adsorbed OH) and CH stretching modes (from oleic acid ligands). The sample was prepared in the KBr pellet form after baking the nanowire sample at 430 K in ultra-high vacuum. The spectrum was taken under inert N_2 environment. **b** Relaxed structure for the 1.6-nm $BaTiO_3$/OH system obtained from our DFT calculations. Barium, titanium, oxygen, and hydrogen atoms are represented by *cyan*, *blue*, *red*, and *gray*, respectively. Displacements from perfect perovskite positions are shown by *arrows* (scaled up by a factor of 7). Reprinted with permission from Ref. [34]. Copyright 2006 American Chemical Society

We note here that molecular adsorption-mediated ferroelectricity was observed and reported in a separate series of theoretical and experimental investigations carried out on ultra-thin films in a controlled atmosphere involving probing of ferroelectric distortions using X-ray reflectivity [30, 32, 62]. More recently, in a separate series of experiments and calculations involving thin films, Li et al. [63] proposed an interesting mechanism for molecular adsorption along ferroelectric surfaces by which molecules remain trapped in a physisorption energy well, under the influence of the surrounding ferroelectric domain state, site-independently. While many species quickly desorb from the surface, molecules that migrate to an active site, most commonly an oxygen vacancy, lead to chemisorption and bond formation. Scanning probe techniques, such as scanning surface potential microscopy (SSPM) and piezoresponse force microscopy (PFM), are sensitive to adsorbed species along a ferroelectric surface, as they indicate finite differences in the domain response as a function of adsorbed species. DFT simulation results were used in Ref. [63] to demonstrate the remarkable effectiveness of molecular adsorbates as screening agents. Here again, selection of oleate ligands left the electropositive HCO fragments preferring the anion species, while the electronegative species HCOO preferred the cation sites. Depending on the presence of electronegative or electropositive adsorbates, bulk-like ferroelectricity was demonstrated for positive and negative polarizations, respectively. These results are in stark contrast to those found for ferroelectric films [14] sandwiched between two metallic and oxide electrodes, which do not exhibit ferroelectric stability at comparable length scales (<1 nm).

Multi-component ferroelectric nanostructures

Recently, the effects of nanoparticle shape on ferroelectric stability and the possibility of new ferroelectric phases have attracted considerable attention, including recent theoretical [15] and experimental evidence for toroidal behavior in ferroelectric nanostructures [64], theoretical [65–67] and experimental [68–70] findings relating to the role of surface tension-induced stress in mitigating the depolarizing field and enhancing axial polarizations via electrostrictive coupling to surface stress [71]. We close by remarking that our group recently has been investigating the effect of finite curvature on evolution of T_C and polarization along in the smallest (radial) direction within ultra-thin shells. Our group has developed a method for producing nanowires each comprises a noble-metal core (e.g., Au) and a ferroelectric oxide perovskite shell, e.g., $PbZr_{0.52}Ti_{0.48}O_3$ (PZT). These multi-component nanowires (Fig. 7) are obtained via a combination of template-assisted growth of nanotubes and electrochemical deposition [72, S.S. Nonnenmann et al., unpublished]. X-ray diffraction, TEM, and Raman analysis indicate that each nanowire consists of a tetragonal PZT nano-shell enclosing an Au nanowire core [72, S.S. Nonnenmann et al., unpublished]. Proximal probing of the ferroelectric switching of individual nano-shells in their finite thickness direction exhibit a markedly different finite-thickness dependence as compared with planar PZT. Significantly, a nearly ~300% enhancement in the ferroelectric polarizations as seen by piezoresponse force microscopy [73] observed in ultra-thin shells of high curvature is supported by calculation results using a radial strain-renormalized Landau–Ginzburg approach to the free energy of ferroelectric polarizations oriented outward or inward normal to the shell surface [72, S.S. Nonnenmann et al., unpublished]. Measured giant ferroelectric piezoelectric responses and finite-curvature-dependent offsets in ferroelectric switching are consistent with a theoretical model description incorporating nanoscale curvature-dependent polarization profiles. In enhancing properties along the smallest dimension, cylindrical nanoshell-based devices possessing finite-curvature-driven strain gradients represent a model system for circumventing finite-size scaling limitations within nanostructured ferroelectric capacitors and for evaluating the effects of surface chemical environment on ferroelectric stability. Moreover, the combination of strain- and strain-gradient-mediated ferroelectricity and the interplay of surface chemical environment with ferroelectric polarizations and their orientations in ultra-narrow diameter nanowires and nanotubes can be expected to further expand the range of interest and applicability of these functional nanostructured materials.

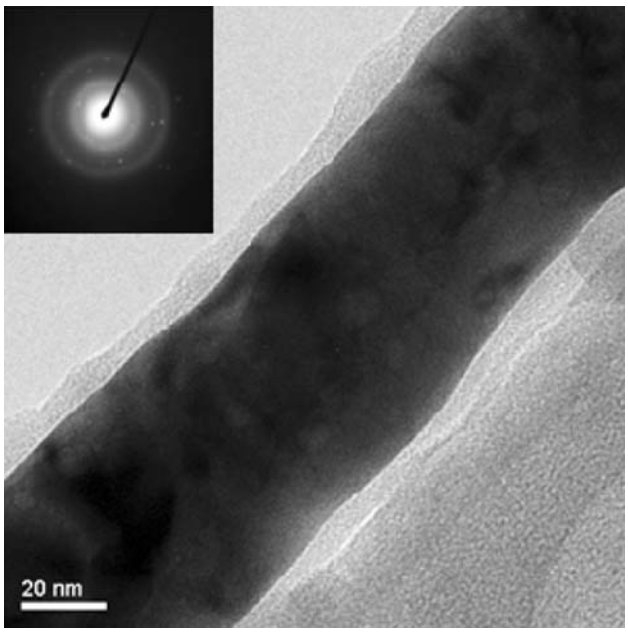

Fig. 7 Transmission electron micrograph of a representative individual Au core, PZT shell nanowire produced as described in the main text; the *inset* is a selected area electron diffraction pattern collected from this nanowire. Au-core, PZT-shell nanowires possessing shell thicknesses ranging from ~7 to more than 30 nm, and shell outer diameters from 30 to ~200 nm have been produced

Acknowledgements The authors thank H. Park, J. J. Urban, W. S. Yun, L. Ouyang, A. M. Rappe, A. Kolpak and I. Grinberg, E. M. Gallo, O. D. Leaffer, M. T. Coster, R. S. Joseph, C. L. Johnson, and G. R. Soja for collaborative contributions to this study, and S. P. Alpay, A. Morozovska, T. McGuckin and S. L. Moskow for helpful additional technical discussions and support. The authors acknowledge support for this study from the Materials Sciences Division of the U. S. Army Research Office under Award No. W911NF-08-1-0067.

References

1. Scott JF, Fan HJ, Kawasaki S, Banys J, Ivanov M, Krotkus A, Macutkevic J, Blinc R, Laguta VV, Cevc P, Liu JS, Kholkin AL (2008) Nano Lett 8:4404
2. Scott JF (2007) Science 315:954
3. Ramesh R, Spaldin NA (2007) Nat Mater 6:21
4. Huang L, Chen Z, Wilson JD, Banerjee S, Robinson RD, Herman I, Laibowitz R, O'Brien S (2006) J Appl Phys 100:034316
5. Ramadan T, Levy M, Osgood RM (2000) Appl Phys Lett 76:1407
6. Scott JF, Morrison FD, Miyake M, Zubko P, Lou X, Kugler VM, Rios S, Zhang M (2005) J Am Ceram Soc 88:1691
7. Rüdiger A, Waser R (2008) J Alloys Compd 449:2
8. Gruverman A, Kholkin A (2006) Rep Prog Phys 69:2443
9. Scott JF, Paz de Araujo C (1989) Science 246:1400
10. Mitsui T, Furuichi J (1953) Phys Rev 90:193
11. Roytburd AL (1976) Phys Status Solidi A 37:329
12. Wang CL, Smith SRP (1995) J Phys: Condens Matter 7:7163
13. Bratkovsky AM, Levanyuk AP (2005) Phys Rev Lett 94:107601
14. Junquera J, Ghosez P (2003) Nature 422:506

15. Naumov I, Fu H, Bellaiche L (2004) Nature 432:737
16. Ishibashi Y, Orihara H (1992) Jpn J Appl Phys 61:4650
17. Alpay SP, Roytburd AL (1998) J Appl Phys 83:4714
18. Pertsev NA, Zembilgotov AG, Tagantsev AK (1998) Phys Rev Lett 80:1988
19. Bratkovsky AM, Levanyuk AP (2000) Phys Rev B 61:15042
20. O'Neill D, Bowman RM, Gregg JM (2000) Appl Phys Lett 77:1520
21. Akdogan EK, Safari A (2007) J Appl Phys 101:064114
22. Akdogan EK, Safari A (2007) J Appl Phys 101:064115
23. Choi KJ, Biegalski M, Li YL, Sharan A, Schubert J, Uecker R, Reiche P, Chen YB, Pan XQ, Gopalan V, Chen LQ, Schlom DG, Eom CB (2004) Science 306:1005
24. Warusawithana MP, Cen C, Sleasman CR, Woicik JC, Li Y, Kourkoutis LF, Klug JA, Li H, Ryan P, Wang LP, Bedzyk M, Muller DA, Chen LQ, Levy J, Schlom DG (2009) Science 324:367
25. Garcia V, Fusil S, Bouzehouane K, Enouz-Vedrenne S, Mathur ND, Barthelemy A, Bibes M (2009) Nature. doi:10.1038/nature08128
26. Haeni JH, Irvin P, Chang W, Uecker R, Reiche P, Li YL, Choudhury S, Tian W, Hawley ME, Craigo B, Tagantsev AK, Pan XQ, Streiffer SK, Chen LQ, Kirchoefer SW, Levy J, Schlom DG (2005) Nature 430:758
27. Dawber M, Lichtensteiger C, Cantoni M, Veithen M, Ghosez P, Johnston K, Rabe KM, Triscone JM (2005) Phys Rev Lett 95:177601
28. Bousquet E, Dawber M, Stucki N, Lichtensteiger C, Hermet P, Gariglio S, Triscone JM, Ghosez P (2008) Nature 452:732
29. Mantese JV, Alpay SP (2005) Graded ferroelectrics, transpacitors, and transponents. Springer, New York
30. Fong DD, Stephenson GB, Streiffer SK, Eastman JA, Auciello O, Fuoss PH, Thompson C (2004) Science 304:1650
31. Tybell T, Ahn CH, Triscone JM (1999) Appl Phys Lett 75:856
32. Fong DD, Kolpak AM, Eastman JA, Streiffer SK, Fuoss PH, Stephenson GB, Thompson C, Kim DM, Choi KJ, Eom CB, Grinberg I, Rappe AM (2006) Phys Rev Lett 96:127601
33. Urban JJ, Spanier JE, Ouyang L, Yun WS, Park H (2003) Adv Mater 15:423
34. Spanier JE, Kolpak AM, Urban JJ, Grinberg I, Ouyang L, Yun WS, Rappe AM, Park H (2006) Nano Lett 6:735
35. Rüdiger A, Schneller T, Roelofs A, Tiedke S, Schmitz T, Waser R (2005) Appl Phys A 80:1247
36. Alexe M, Hesse D (2006) J Mater Sci 41:1. doi:10.1007/s10853-005-5912-x
37. Xia Y, Yang P, Sun Y, Wu Y, Mayers B, Gates B, Yin Y, Kim F, Yan H (2003) Adv Mater 15:353
38. Yoon S, Baik S, Kim MG, Shin N (2006) J Am Ceram Soc 89:1816
39. Hoshina T, Kakemoto H, Tsurumi T, Wada S, Yashima M (2006) J Appl Phys 99:054311
40. O'Brien S, Brus LE, Murray CB (2001) J Am Chem Soc 123:12085
41. Zhao J, Wang X, Li L, Wang X, Li Y (2008) Ceram Int 34:1223
42. Whang D, Jin S, Wu Y, Lieber CM (2003) Nano Lett 3:1255
43. Masuda H, Fukuda K (1995) Science 268:1466
44. Sadasivan V, Richter CP, Menon L, Williams PF (2005) AIChE Journal 51:649
45. Steinhart M, Wendorff JH, Greiner A, Wehrspohn RB, Nielsch K, Schilling J, Choi J, Goesele U (2002) Science 296:1997
46. Urban JJ, Yun WS, Gu Q, Park H (2002) J Am Chem Soc 124:1186
47. Hernandez BA, Chang KS, Fisher ER, Dorhout PK (2002) Chem Mater 14:480
48. Luo Y, Szafraniak I, Zakharov ND, Nagarajan V, Steinhart M, Wehrspohn RB, Wendorff JH, Ramesh R, Alexe M (2003) Appl Phys Lett 83:440
49. Morrison FD, Ramsay L, Scott JF (2003) J Phys-Condens Matter 15:L527
50. Park TJ, Mao Y, Wong SS (2004) Chem Commun 23:2708
51. Zhao L, Steinhart M, Yu J, Gösele U (2006) J Mater Res 21:685
52. Cheng JY, Ross CA, Smith HI, Thomas EL (2006) Adv Mater 18:2505
53. Evans PR, Zhu X, Baxter P, McMillen M, McPhillips J, Morrison FD, Scott JF, Pollard RJ, Bowman RM, Gregg JM (2007) Nano Lett 7:1134
54. Lee W, Han H, Lotnyk A, Schubert MA, Senz S, Alexe M, Hesse D, Baik S, Gösele U (2008) Nat Nanotechnol 3:402
55. Yun WS, Urban JJ, Gu Q, Park H (2002) Nano Lett 2:447
56. Kalinin SV, Bonnell DA (2000) J Appl Phys 87:3950
57. Noma T, Wada S, Yano M, Suzuki T (1996) J Appl Phys 80:5223
58. Abicht HP, Voltzke D, Schneider R, Woltersdorf J, Lichtenberger O (1998) Mater Chem Phys 55:188
59. Wegmann M, Watson L, Hendry A (2004) J Am Ceram Soc 87:371
60. Sun Q, Reuter K, Scheffler M (2003) Phys Rev B 67:205424
61. Reuter K, Scheffler M (2003) Phys Rev Lett 90:046103
62. Wang RV, Fong DD, Jiang F, Highland MJ, Fuoss PH, Thompson C, Kolpak AM, Eastman JA, Streiffer SK, Rappe AM, Stephenson GB (2009) Phys Rev Lett 102:047601
63. Li D, Zhao MH, Garra J, Kolpak AM, Rappe AM, Bonnell DA, Vohs JM (2008) Nat Mater 7:473
64. Rodriguez BJ, Gao XS, Liu LF, Lee W, Naumov II, Bratkovsky AM, Hesse D, Alexe M (2009) Nano Lett 9:1127
65. Morozovska AN, Eliseev EA, Glinchuk MD (2007) Phys B 387:358
66. Morozovska AN, Glinchuk MD, Eliseev EA (2007) Phase Transit 80:71
67. Morozovska AN, Glinchuk MD, Eliseev EA (2007) Phys Rev B 76:014102
68. Yadlovker D, Berger S (2005) Phys Rev B 71:184112
69. Wang Z, Hu J, Yu MF (2006) Appl Phys Lett 89:263119
70. Alexe M, Hesse D, Schmidt V, Senz S, Fan HJ, Zacharias M, Gösele U (2006) Appl Phys Lett 89:172907
71. Damjanovic D, Budimir M, Davis M, Setter N (2006) J Mater Sci 41:65. doi:10.1007/s10853-005-5925-5
72. Nonnenmann SS, Leaffer OD, Gallo EM, Coster MT, Joseph RS, Spanier JE (2009) Ferroelectric properties of co-axial noble-metal/oxide core/shell perovskite nanowires. MRS fall meeting, Boston MA, Poster C9.5
73. Gruverman A, Kalinin SV (2006) J Mater Sci 41:107. doi:10.1007/s10853-005-5946-0